ACS APPLIED MATERIALS & INTERFACES

www.acsami.org

Research Article

Multifunctional Cellulose Nanocrystals as a High-Efficient Polysulfide Stopper for Practical Li−S Batteries

Jie Liu, Yanyan Li, Yuxue Xuan, Liujiang Zhou, Dong Wang, Zhenwei Li, Haifeng Lin, Sergei Tretiak, Hui Wang,* Lei Wang,* Ziyang Guo, and Shanqing Zhang*

Cite This: *ACS Appl. Mater. Interfaces* 2020, 12, 17592−17601

Read Online

ACCESS | Metrics & More | Article Recommendations | Supporting Information

ABSTRACT: Because of the severe shuttle effect of polysulfides, achieving durable Li−S batteries is still a great challenge, especially under practical operation conditions including the high sulfur content, high loading, and high operation temperature. Herein, for the first time, low-cost, eco-friendly, and hydrophilic cellulose nanocrystals (CNCs) are proposed as a multifunctional polysulfide stopper for Li−S batteries with high performance. CNCs display an intrinsically high aspect ratio and a large surface area and contain a large amount of hydroxyl groups offering a facile platform for chemical interactions. Density functional theory calculations suggest that the electron-rich functional groups on CNCs deliver robust binding energies with polysulfides. In this work, CNCs not only firmly confine sulfur and polysulfides in the cathode as a robust binder, but also further hinder polysulfide shuttling to the Li anode as a polysulfide stopper on a separator. Consequently, the as-prepared Li−S batteries demonstrate outstanding cycling performance even under the conditions of high sulfur content of 90 wt % (63 wt % in the cathode), high loading of 8.5 mg cm^{-2}, and high temperature of 60 °C. These results sufficiently demonstrate that CNCs have significant application potential in Li−S battery technologies.

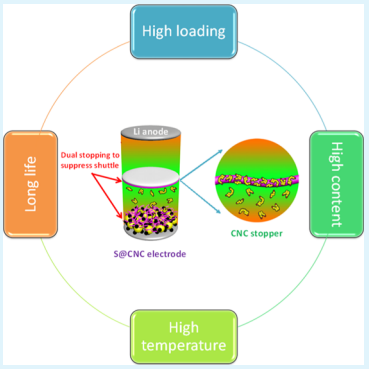

KEYWORDS: *Li−S battery, cellulose nanocrystals, polysulfide stopper, practical condition, high loading*

INTRODUCTION

Owing to the high energy density of 2600 W h Kg^{-1}, Li−S batteries have been considered as one of the most promising energy storage devices, and subsequently have been attracting a tremendous amount of attention.[1−4] However, during the charge and discharge processes, soluble long-chain lithium polysulfides (Li_2S_x, $4 \leq x \leq 8$) are formed and cause a severe shuttle effect, leading to poor cycling stability.[5−8] This calls for efficient host materials to immobilize lithium polysulfides, a crucial component for making durable Li−S batteries.

Polymers with abundant electron-rich functional groups (e.g., hydroxyl, carboxyl, and amino), which possess strong affinity for lithium polysulfides, have been demonstrated to be a class of potential host materials.[9−22] In particular, multifunctional polymer binders have generated much research interest, as they can not only bind sulfur and conductive carbon to the current collector but also chemically constrain polysulfides in the cathode. Subsequently, various polymer binders have been investigated to replace the commercial polyvinylidene fluoride (PVDF) binder, including poly(vinylpyrrolidone),[9] carrageenan,[10] guar gum−xanthan gum network binder,[11] conductive double-chain polymer network binder,[12] and polyamidoamine dendrimers.[13] Another potential application of polymers in Li−S batteries is using them to modify separators/interlayers and hinder the polysulfide shuttle, such as the Nafion-based ion-selective separator,[16−18] tertiary amine layer-modified polypropylene (PP) separator,[19] and gum arabic-carbon nanofiber interlayer.[20] Compared with other host materials such as metal compounds, polymer host materials possess low density, causing a smaller mass increase of inactive components. Furthermore, the metal compound host materials usually need a binder to bind them to the electrode or separator, further decreasing the sulfur content. Although significant progress has been made in improving the electrochemical performance of Li−S batteries by exploiting polymer host materials, the shuttle effect still remains the main bottleneck under practical working conditions including the high sulfur content, high loading, and high operation temperature. Therefore, it is still a critical need to further explore promising polymer host materials to solve the above key challenge for Li−S batteries.

Cellulose, the most abundant biomass in the world, is a linear syndiotactic homopolymer of β-(1→4)-glycosidic bonds linked D-glucopyranose units. Cellulose has been exploited to prepare porous separators for suppressing Li dendrite

Received: February 3, 2020
Accepted: February 24, 2020
Published: February 24, 2020

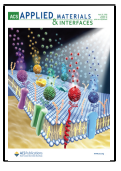

https://dx.doi.org/10.1021/acsami.0c00537
ACS Appl. Mater. Interfaces 2020, 12, 17592−17601

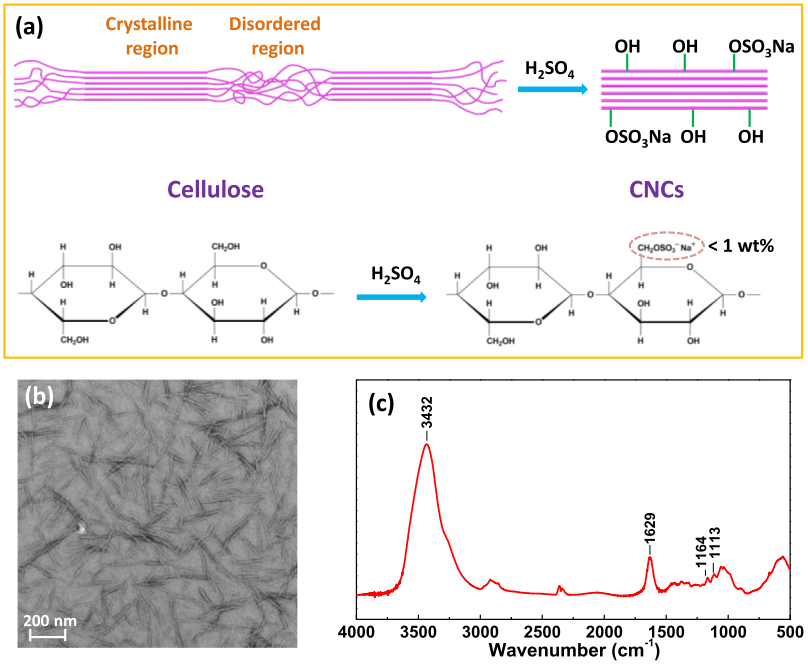

Figure 1. (a) Schematic illustration of the preparation process of CNCs by acid hydrolysis wiping off the disordered regions of cellulose; (b) TEM image of CNCs; and (c) FTIR spectrum of CNCs.

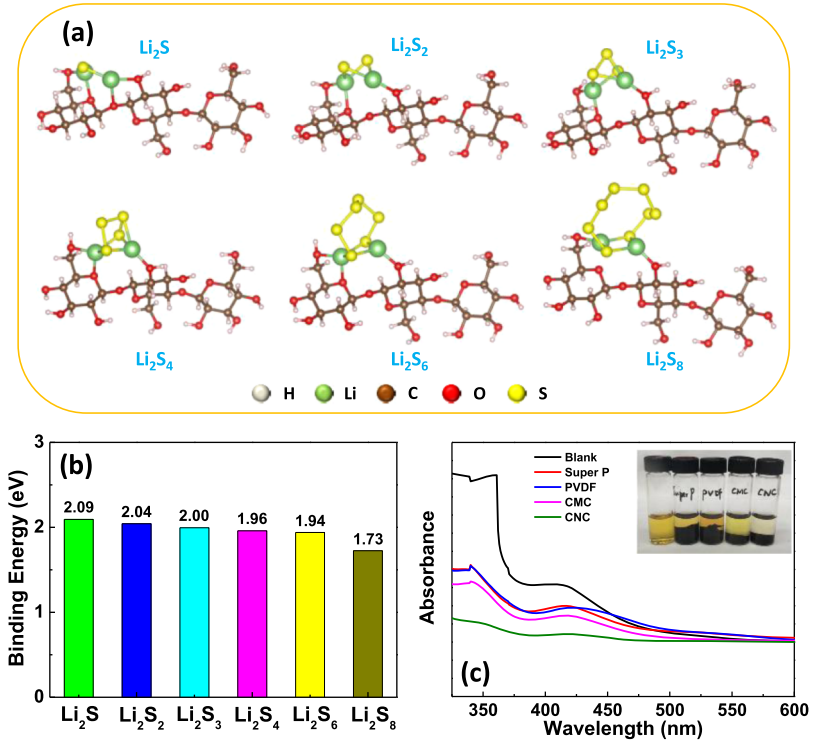

Figure 2. (a) Optimized structures of lithium polysulfides (Li_2S, Li_2S_2, Li_2S_3, Li_2S_4, Li_2S_6, and Li_2S_8) at six different lithiation conformations of CNCs. In the models, the back structures of CNCs were mimicked by three constitutional units, in which the $SO_3^-Na^+$ ligand was substituted by the H atom because of its low concentration (<1 wt %). (b) The corresponding adsorption binding energies between lithium polysulfides and CNCs. (c) UV−vis spectra of polysulfide solutions after polysulfide adsorption tests of Super P, PVDF, CMC, and CNCs, showing the robust affinity of CNCs for polysulfides. The inset in (c) shows the digital photo of the polysulfide solutions, showing the solution color change during the polysulfide adsorption tests.

formation in the previous literature, which is mainly because of the homogeneous distribution of nano-channels giving a uniform current density, good wettability, and electrolyte uptake.[23−25] Upon acid hydrolysis, cellulose yields highly crystalline rod-like hydrophilic particles at the nanoscale level [i.e., cellulose nanocrystals (CNCs)],[26,27] as shown in Figure 1a. CNCs display an intrinsically high aspect ratio and a large surface area, making them promising nanomaterials. Specifi-

https://dx.doi.org/10.1021/acsami.0c00537
ACS Appl. Mater. Interfaces 2020, 12, 17592−17601

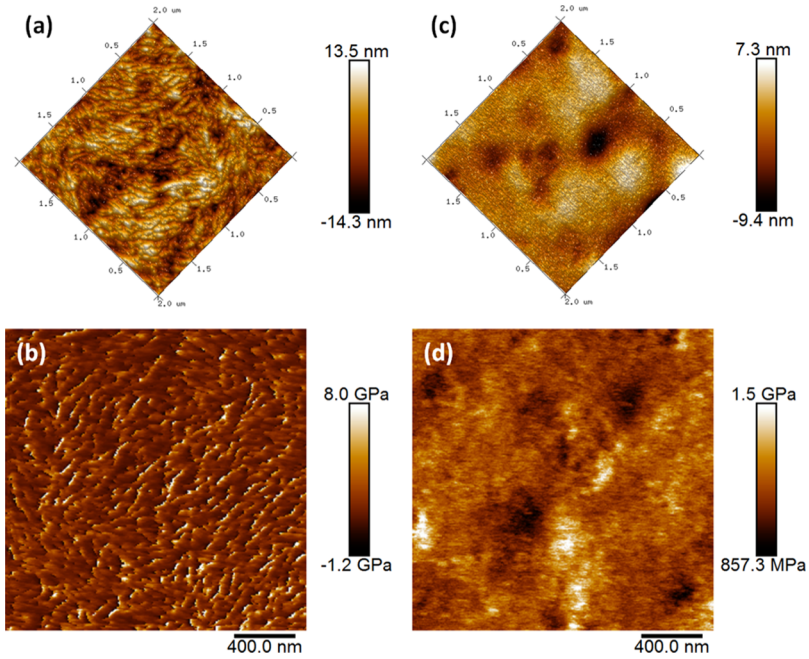

Figure 3. (a,c) AFM topography and (b,d) quantitative high-resolution DMT modulus (Young's modulus) images measured by PeakForce Quantitative NanoMechanics (QNM) technique according to the DMT model of CNCs and CMC, respectively.

cally, the large interfacial area and strong interactions among the polymer matrix give rise to nano-confinement effects, enabling substantial improvement of mechanical properties.[28] CNCs can bear extraordinary bending strength and modulus, estimated to be ~10 and 150 GPa, respectively, which are comparable in magnitude to those of carbon nanotubes.[29] On the other hand, as displayed in Figure 1a, CNCs contain abundant hydroxyl groups, which can offer a facile platform for chemical modification and interaction.[30,31]

Herein, for the first time, CNCs were exploited as a high-efficiency and promising polysulfide stopper for high-performance Li−S batteries. CNCs can prevent sulfur and polysulfides from dissolving out the cathode as a multifunctional binder, and further hinder the shuttling of polysulfides to the Li anode as a stopper on the separator. Because of the robust mechanical properties and strong affinity of CNCs, the Li−S battery has a stable cycling performance with a long lifespan, even with a high sulfur content of up to 90 wt % (63 wt % in the cathode), a high loading of 8.5 mg cm^{-2}, and being operated at a high temperature of 60 °C. These results led us to believe that CNCs have significant application potential in Li−S battery technology.

RESULTS AND DISCUSSION

The CNCs were supplied by CelluForce Inc., Canada, and used as received, with a specific surface area of approximately 500 m^2 g^{-1}. Figures 1b and S1 demonstrate that the as-obtained CNCs are composed of rod-like shaped nanoparticles with an average length of 148.52 nm and an average diameter of 8.30 nm. The Fourier transform infrared (FTIR) spectrum of CNCs (Figure 1c) displays a broad absorption band at 3432 cm^{-1} reflecting the O−H vibration mode, a band at 1164 cm^{-1} assigned to the asymmetrical bridge C−O−C stretching in the glycosidic bond, and a peak at 1113 cm^{-1} corresponding to the stretching of the glucopyranose unit.[32,33] These abundant oxygen-containing functional groups with lone pair of electrons can act as Lewis bases to form strong affinity for the Lewis acids of terminal Li atoms in lithium polysulfides, by which lithium polysulfides are thus firmly immobilized on the polymers.[34] The chemisorption ability of CNCs to lithium polysulfides was investigated using density functional theory (DFT) calculations (Figure 2a,b). The simulations suggest that the constitutional units of CNCs can bind to Li_2S, Li_2S_2, Li_2S_3, Li_2S_4, Li_2S_6, and Li_2S_8 with energies of 2.09, 2.04, 2.00, 1.96, 1.94, and 1.73 eV, respectively, which are much higher than that of PVDF with Li−$S^{\bullet}$ species (0.75 eV).[35] The strong chemisorption of CNCs with polysulfides makes CNCs promising host materials for Li−S batteries. Polysulfide adsorption tests can visually show the stronger affinity of CNCs to lithium polysulfides. As displayed in Figure 2c, the Li_2S_6 solution with CNCs discolors obviously because of the strong adsorption of CNCs to polysulfides; while the solutions with Super P, PVDF, and carboxymethyl cellulose (CMC) still remain orange, suggesting a weak adsorption. Meanwhile, the UV−vis spectra of the polysulfide solutions after adsorption tests quantitatively demonstrate the high-efficient chemisorption ability of CNCs to lithium polysulfides, reflected by the significant concentration decrease of polysulfides in the solution.

Figure S2 demonstrates that the hydrophilic CNCs are highly dispersed in water to form a viscous aqueous suspension, whose viscosity is comparable to the traditional CMC binder, suggesting that CNCs have potential to be applied as a binder. The bending experiment of the sulfur electrode with the CNC binder (Figure S3) clearly shows good adhesive property of the CNC binder on the current collector. For a binder of the Li−S battery, strong mechanical properties are required to accommodate the large volume change (~80%) from S to Li_2S and maintain the integrity of the electrode during cycling.[15,21] Atomic force microscopy (AFM) test was carried out to evaluate the mechanical strength of the CNC binder. Quantitative high-resolution Young's modulus mapping was measured by PeakForce Quantitative NanoMechanics (QNM) technique according to the Derjaguin−Muller−

https://dx.doi.org/10.1021/acsami.0c00537
ACS Appl. Mater. Interfaces 2020, 12, 17592−17601

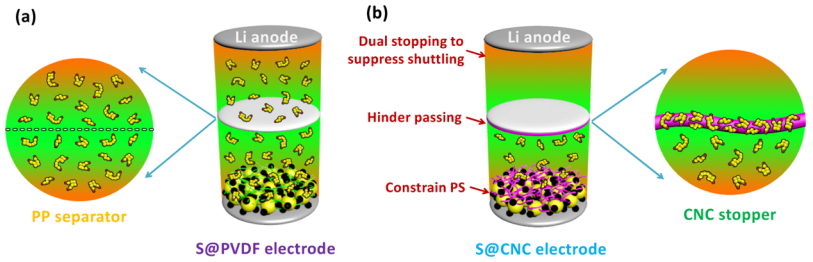

Figure 4. Schematic presentation: (a) Li−S battery using a PVDF binder and a PP separator with a severe shuttle effect; (b) Li−S battery with a CNC binder and a CNC polysulfide stopper on a PP separator to efficiently suppress the shuttle effect.

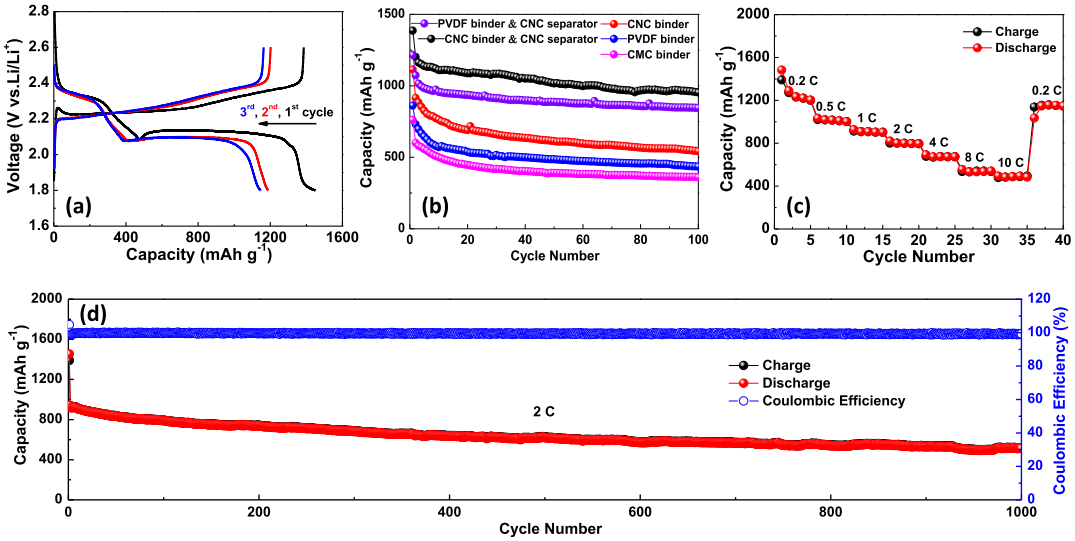

Figure 5. (a) Charge−discharge curves of the Li−S battery with a CNC binder and a CNC-coated separator; (b) comparison of the cycling performances of the Li−S batteries using different polymers at 0.5 C (the first cycle was at 0.2 C); (c) rate property; and (d) extended cycling performance at 2 C (the first cycle was at 0.2 C) of the Li−S battery using a CNC binder and a CNC-coated separator.

Toporov (DMT) model. For comparison, the traditional cellulose-based binder CMC was also tested. The obtained AFM topography and the corresponding DMT modulus (Young's modulus) images of the CNC binder and the CMC binder are displayed in Figure 3. Figure 3a,c demonstrates that the CNC binder film is more rough with a larger surface area for chemical interactions because of the crystalline characteristic. Importantly, as shown in Figure 3b,d, the CNC binder possesses higher Young's modulus to accommodate the stress caused by the large volume change, and thus maintains an integrated conductive network in the electrode during cycling.[14]

According to the above discussion, in the current study, the CNCs are applied not only as a multifunctional binder to prevent the sulfur and polysulfides from dissolving out the cathode, but also as a polysulfide stopper on the separator to further hinder polysulfide migration to the Li anode, as indicated in Figure 4. Resulting from the dual stopping of CNCs, the shuttle effect can be remarkably suppressed. Galvanostatic charge−discharge cycling tests were conducted to evaluate the electrochemical performance of Li−S batteries using CNCs as the binder and the polysulfide stopper. The sulfur cathode is composed of the S/Ketjen black (S/KB) composite, carbon nanotubes, and a CNC binder with a mass ratio of 70:15:15, respectively. The scanning electron microscopy (SEM) image and the elemental mapping of the as-prepared sulfur cathode (Figure S4) indicate that sulfur and carbon are uniformly distributed in the cathode. The CNC-coated separator is obtained as the polysulfide stopper by homogeneously covering a layer of the CNC/KB composite on the commercial PP separator, as shown in Figure S5. With KB as a conductive additive, the CNC-coated separator can work as a second current collector, making the absorbed polysulfides to continually transform into final products. The coating thickness is measured to be 6.5 μm from the cross-section SEM image of the CNC-coated separator (Figure S6). As shown in Figure S7, the bending experiment of the CNC-coated separator demonstrates that the CNC-coated separator possesses acceptable flexibility. Figure 5a displays the typical charge−discharge curves of the Li−S battery, that is, the conversion of cyclo-S_8 to soluble long-chain polysulfides (Li_2S_x, $4 \le x \le 8$) at 2.35 V and further reduction to Li_2S_2/Li_2S at 2.13 V.[36−38] The redox peaks in cyclic voltammetry (CV) curves in Figure S8 agree very well with the charge−discharge potential platforms. The cycling performances of the as-prepared Li−S batteries at 0.5 C are displayed in Figure 5b. Owing to the robust mechanical properties and strong affinity of CNCs, the sulfur cathode with the CNC binder shows superior cycling performance than that with traditional PVDF and CMC binders (543 mA h g^{-1} vs 436 mA h g^{-1} and 362 mA h g^{-1} after 100 cycles). Benefiting from the dual constraint of CNCs to polysulfides, the Li−S battery with CNCs as the binder and the polysulfide stopper can show a further improved cycling performance giving a capacity as high as 954 mA h g^{-1} after 100 cycles. It should be mentioned that the Li−S battery possesses quite high Coulombic efficiency of

https://dx.doi.org/10.1021/acsami.0c00537
ACS Appl. Mater. Interfaces 2020, 12, 17592−17601

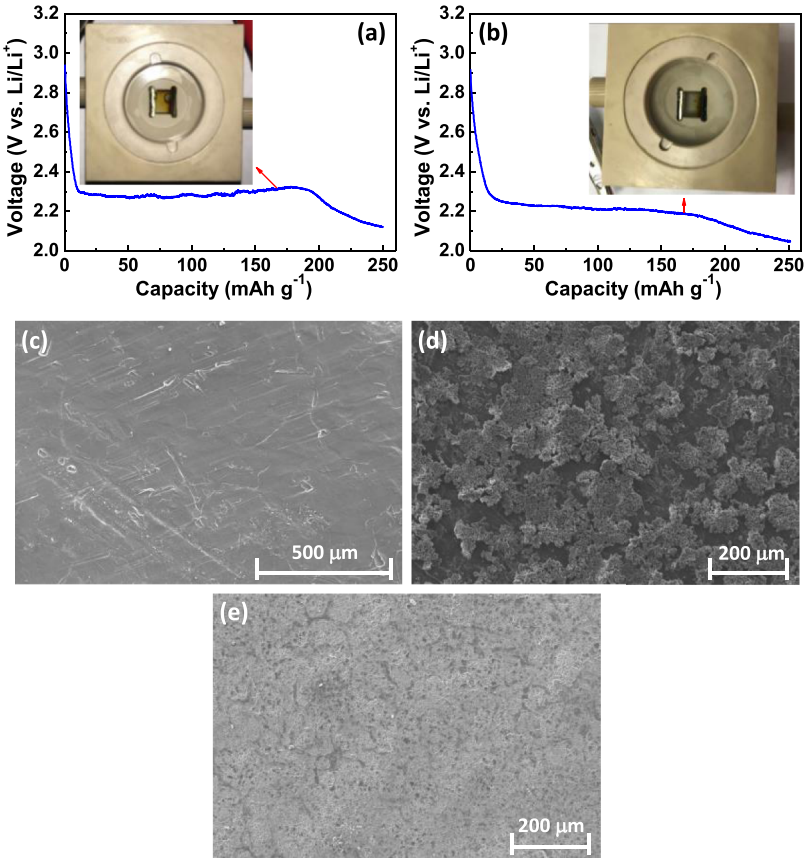

Figure 6. Discharge curves at 0.2 C of an in situ cell (a) with a PVDF binder and a PP separator and (b) with a CNC binder and a CNC-coated separator. Insets show the digital photos of the in situ cell after discharging for 0.5 h. SEM images of the Li anode (c) before cycling and after 50 cycles obtained from the Li−S battery (d) with a PVDF binder and a PP separator and (e) with a CNC binder and a CNC-coated separator.

99.97% after 100 cycles (Figure S9), suggesting that the shuttle effect is dramatically suppressed. The Li−S battery using the PVDF binder and the CNC-coated separator was also tested. It shows much improved capacity (845 mA h g^{-1} after 100 cycles) compared to the Li−S battery using the PVDF binder and the PP separator, indicating the important effect of the CNC-coated separator. However, its cycling performance is still inferior to the battery with the CNC binder and the CNC-coated separator, indicating that the CNC binder also plays an important role in affixing polysulfides to the cathode. Unusually, the binder amount in the electrode is low (≤15 wt %), leading to limited chemical adsorption. Therefore, in this work, CNCs are applied not only as a robust binder to firmly confine sulfur and polysulfides in the cathode, but also as a polysulfide stopper on a separator to further hinder polysulfide shuttling to the Li anode. Figure 5c demonstrates that the Li−S battery with the CNC binder and the CNC-coated separator also exhibits an outstanding rate property, delivering a capacity of 487 mA h g^{-1} at 10 C. In the long-term test (Figure 5d), the Li−S battery with the CNC binder and the CNC-coated separator still shows excellent cycling stability with a high Coulombic efficiency of 99.28% and a capacity of 514 mA h g^{-1} after 1000 cycles at 2 C, corresponding to a very low capacity fading of 0.045% per cycle from the second cycle.

The improved electrochemical properties are mainly because of the robust chemical adsorption of CNCs to polysulfides. As discussed in Figure 2, the DFT calculations and polysulfide adsorption experiments have demonstrated the strong adsorption ability of CNCs. An in situ cell is assembled to directly and visually observe the important effect of the CNC binder and the CNC-coated separator on hindering the shuttle effect. Figure 6a shows the discharge curve of an in situ cell with a PVDF binder and a PP separator and a digital photo after discharging for 0.5 h (inset). It shows that the PVDF binder and the PP separator possess very poor ability to hinder the polysulfide movement to the Li anode with an orange electrolyte. However, in Figure 6b, an in situ cell with a CNC binder and a CNC-coated separator displays much improved ability to restrict the polysulfides within the cathode side with a colorless electrolyte because of the robust affinity of CNCs for polysulfides. The morphology changes of the Li anodes in the Li−S batteries after cycling are also compared. Figure 6c shows that the fresh Li anode possesses a smooth surface. After 50 cycles, the Li anode in the Li−S battery with a PVDF binder and a PP separator becomes very rough (Figure 6d). It seems that the heavy sediment is on the Li anode, such as Li_2S and Li_2S_2, which is formed because of the shuttle effect.[39] Whereas the Li anode in the Li−S battery with a CNC binder and a CNC-coated separator has a relatively smooth surface (Figure 6e), suggesting that the shuttle effect is effectively hindered. For practical application of the Li−S battery, stable Li anodes are critically needed for further improved performance and safety.[24,40]

To further evaluate the capability of CNCs to suppress the shuttle effect, more rigorous test conditions were carried out. It is crucial to increase the level of sulfur content in relation to the energy density of the whole Li−S battery.[41,42] However, the high-content sulfur in the cell typically causes much more

https://dx.doi.org/10.1021/acsami.0c00537
ACS Appl. Mater. Interfaces 2020, 12, 17592−17601

severe shuttle effect, making the high-sulfur-content Li−S battery very difficult to achieve. By using the multifunctional CNCs as both the binder and polysulfide stopper, we fabricated a Li−S battery with a high sulfur content of up to 90 wt % (63 wt % in the cathode). As shown in Figure 7a, the high-sulfur-content Li−S battery displays a long cycling life giving a capacity of 593 mA h g^{-1} after 700 cycles, corresponding to a capacity fade as low as 0.047% per cycle from the second cycle. This is among the best performing Li−S batteries (Table S1). On the other hand, the shuttle effect becomes more serious during cycling at high temperatures, and a more powerful strategy to immobilize the lithium polysulfides is required.[43] In the present study, the high-temperature cycling test was also performed at 60 °C. As displayed in Figure 7b, the Li−S battery, with a sulfur content of 60 wt % in the S/KB composite, still has a stable cycling performance with a high capacity of 896 mA h g^{-1} and a Coulombic efficiency of 99.95% after 100 cycles at 1 C. $LiNO_3$ as an electrolyte additive has been known to effectively suppress the shuttle effect.[44] The Li−S battery without the $LiNO_3$ additive in the electrolyte was also tested. As indicated in Figure 7c, the Li−S battery also shows good cycling stability with a high capacity of 893 mA h g^{-1} and a Coulombic efficiency of 93.7% after 100 cycles at 0.5 C. These results are sufficient evidence that CNCs are excellent host materials for Li−S batteries.

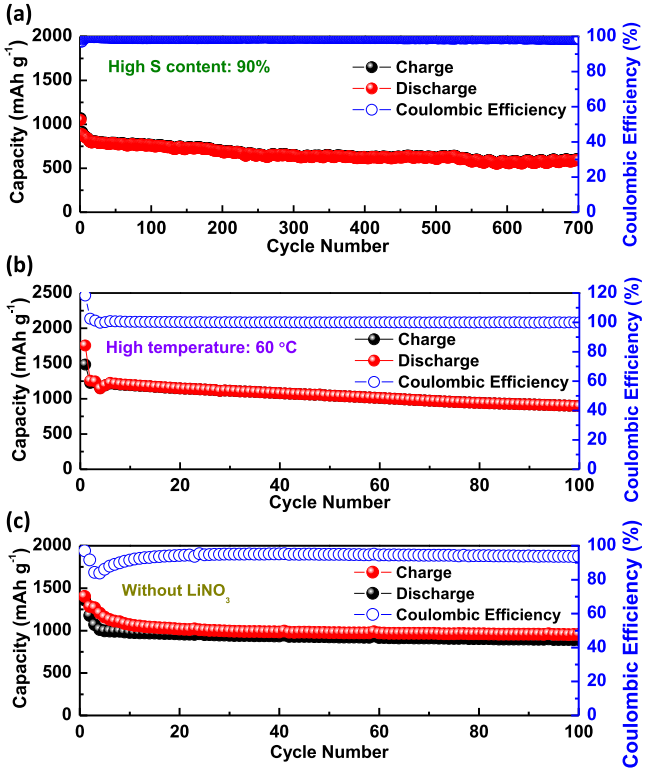

Figure 7. Cycling performance of the Li−S battery with a CNC binder and a CNC-coated separator (a) with a sulfur content as high as 90 wt % (63 wt % in the cathode) at 0.5 C (the first cycle was at 0.2 C), (b) at a high temperature of 60 °C at 1 C (the first cycle was at 0.2 C), and (c) without the $LiNO_3$ additive at 0.5 C (the first cycle was at 0.2 C).

High-loading sulfur electrodes were prepared to achieve a high areal capacity, which is crucial to obtain a high energy density.[45,46] Figure 8a displays the charge−discharge curves of the Li−S battery with a high sulfur loading of 4.1 mg cm^{-2}, showing the typical redox reaction of Li−S batteries with the conversion of cyclo-S_8 to soluble long-chain polysulfides at 2.33 V and further reduction to Li_2S_2/Li_2S at 2.12 V. It also indicates that the high-loading Li−S battery can deliver a high initial discharge capacity of 1284 mA h g^{-1}, corresponding to an areal capacity of 5.3 mA h cm^{-2}. Figure 8b demonstrates that owing to the robust mechanical properties and strong affinity of CNCs, the high-loading Li−S battery show stable cycling performance with a high Coulombic efficiency of 93.90% and a capacity of 726 mA h g^{-1} after 69 cycles, corresponding to an areal capacity of 3.0 mA h cm^{-2}. As the sulfur loading is increased to 8.5 mg cm^{-2}, the Li−S battery can deliver a high initial areal capacity as high as 10.7 mA h cm^{-2}, as shown in Figure 8c. After performing stable cycling for 35 cycles at 1.2 mA cm^{-2}, a high areal capacity of 6.1 mA h

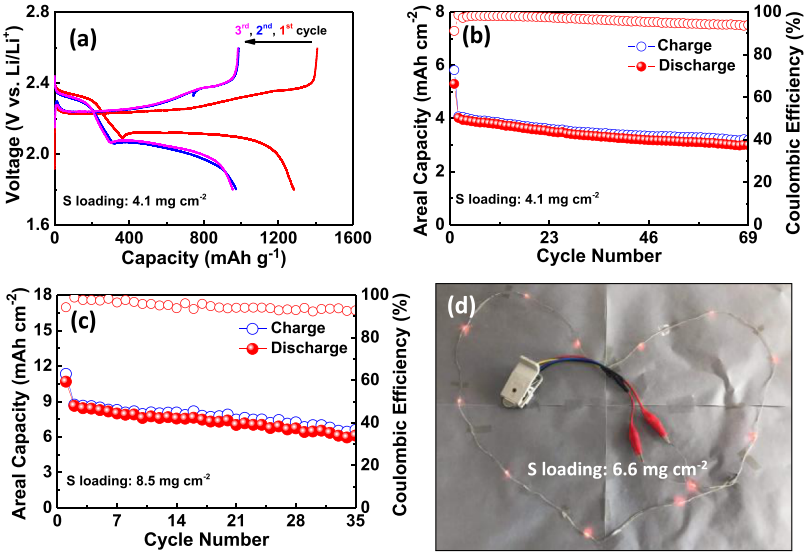

Figure 8. (a) Charge−discharge curves and (b) cycling performance of the Li−S battery with a sulfur loading of 4.1 mg cm^{-2} at 1.2 mA cm^{-2} (the first cycle was at 0.3 mA cm^{-2}); (c) cycling performance of the Li−S battery with a sulfur loading of 8.5 mg cm^{-2} at 1.2 mA cm^{-2} (the first cycle was at 0.3 mA cm^{-2}); and (d) digital photo of the Li−S battery with a sulfur loading of 6.6 mg cm^{-2} to power LED lights.

https://dx.doi.org/10.1021/acsami.0c00537
ACS Appl. Mater. Interfaces 2020, 12, 17592−17601

cm^{-2} with a high Coulombic efficiency of 92.78% can still be obtained. In order to show the practical application potential, a Li−S battery with a high sulfur loading of 6.6 mg cm^{-2} is used to power light-emitting diode (LED) lights. Figure 8d clearly shows that the Li−S battery possesses high energy density to light 12 red LED lights. These results lead us to believe that CNCs have significant application potential in Li−S battery technologies.

CONCLUSIONS

Multifunctional CNCs are explored theoretically and experimentally as high-performance polysulfide host materials, which have inherent advantages of being abundant, low-cost, and hydrophilic. Quantitative high-resolution Young's modulus mappings indicate that CNCs possess robust mechanical strength. DFT calculations and polysulfide adsorption tests clearly demonstrate that CNCs possess strong affinity for lithium polysulfides, attributed to their abundant oxygen-containing functional groups and nanocrystal characteristic. As a consequence, when CNCs are applied as both the binder and polysulfide stopper, the Li−S battery displays excellent cycling stability and rate property. Especially, under rigorous practical conditions including the high sulfur content, high loading, and high operation temperature, the as-prepared Li−S batteries still show outstanding cycling performance, that is, with sulfur content as high as 90 wt % (63 wt % in the cathode), a capacity fade as low as 0.047% per cycle after 700 cycles is obtained; with a high loading of up to 8.5 mg cm^{-2}, an areal capacity as high as 10.7 mA h cm^{-2} is delivered; and being operated at 60 °C, a high capacity of 896 mA h g^{-1} after 100 cycles is achieved. This study provides a novel promising host material to promote the practical application of the Li−S battery.

EXPERIMENTAL SECTION

Material Characterization. SEM images were obtained on a JSM-6390 emission scanning electron microscope, and elemental mapping was obtained using an EDAX Genesis energy dispersive X-ray fluorescence spectrometer. The transmission electron microscopy (TEM) image was obtained on a LEO 912 AB 100 kV energy filtered transmission electron microscope. The FTIR spectrum was recorded on a Nicolet iS50 spectrometer using KBr pellets.

Theoretical Calculations. To investigate the chemisorption ability of CNC molecules toward the Li_2S_x cluster, DFT calculations were carried out using the Gaussian 16 software package[47] under the rB3LYP functional. The 6-31G(d+p) basis set was used for all atoms. The local minima or transition states were determined through vibrational frequency analyses at the same level on optimized geometries. The chemisorption binding energy (E_b) was calculated to describe the affinity of the reducible CNC molecular structure (E_{CNC}) for Li_2S_x (x = 1, 2, 3, 4, 6, and 8) ($E_{Li_2S_x}$) through the energy difference between the CNC/Li_2S_x adsorbed system (E_{Li_2S+PEI}) and the isolated Li_2S_x cluster and the CNC molecule ($E_b = E_{Li_2S_x} + E_{CNC} - E_{Li_2S+PEI}$).

Adsorption Experiments. In a typical process, 100 mg of Super P, 100 mg of PVDF/Super P composite, 100 mg of CMC/Super P composite, and 100 mg of CNC/Super P composite were dispersed in 3 mL polysulfide solution (0.5 mM Li_2S_6 in tetrahydrofuran, THF), respectively. The Li_2S_6 solution was obtained by mixing sulfur and lithium sulfide powders in THF at 50 °C for 12 h under stirring. UV−vis spectra were collected on a METASH UV-8000 spectrometer to quantitatively analyze the chemisorption ability of various polymers.

Mechanical Property Evaluations. AFM (Dimension Icon, Bruker) experiments were carried out in air at room temperature. Young's modulus was obtained through PeakForce QNM technique. First, the probe (SCANASYST-AIR, Bruker) deflection sensitivity was calibrated on a clean and hard sapphire sample. Then, the probe was calibrated with a known-modulus polystyrene by adjusting a suitable force set point of the tip and the tip radius. Finally, using the tip, the samples were measured. The topography and QNM were measured simultaneously in such a way there were 256 × 256 pixels/scan, that is, 65,536 points of the sample were probed and their force curves were obtained. Young's modulus was derived through these obtained force curves based on the DMT model.

Electrochemical Tests. The S/KB composite was fabricated by mixing KB and sulfur powders with a sulfur content of 60 or 90 wt %, and heating them in a sealed Teflon container at 155 °C for 12 h. To prepare the sulfur cathode, the S/KB composite was mixed with multiwalled carbon nanotubes and the CNC binder at a weight ratio of 70:15:15 in deionized water to form a uniform slurry. Then, the slurry was cast onto a carbon-coated Al foil, followed by vacuum drying at 60 °C for 12 h. The CNC-coated separator was obtained by coating the CNC/KB composite at a weight ratio of 2:3 on a commercial PP separator (Celgard 2400) with a doctor-blade coating method, using deionized water as a solvent (a small amount of ethanol was added for wetting). For the electrochemical test, the CR2016 coin cell was assembled in an argon-filled glove box with lithium foil as counter and reference electrodes, a CNC-coated separator or PP separator, and an electrolyte of 1 M lithium bis-(trifluoromethanesulfonyl)imide (LiTFSI) in 1,2-dimethoxyethane and 1,3-dioxolane (1:1 by volume) with 2 wt % $LiNO_3$ as an additive. Galvanostatic charge−discharge cycling tests were carried out on a LAND CT2001A battery testers in a voltage window of 1.8−2.6 V at room temperature or a high temperature of 60 °C. To further demonstrate the important effect of the CNC binder and the CNC-coated separator on hindering the shuttle effect, the cycling performance without the $LiNO_3$ additive was also obtained with the electrolyte/sulfur ratio of about 47 μL mg^{-1}. CV curves were obtained on a CHI760E electrochemical workstation at a scanning rate of 0.1 mV s^{-1} between 1.8 and 2.6 V.

High-Loading Li−S Batteries. The S/Super P composite was fabricated by mixing sulfur and Super P with a mass ratio of 7:3 and heating at 155 °C for 12 h in a sealed Teflon container. The sulfur cathode was prepared by casting a slurry (80 wt % S/Super P composite, 10 wt % KB, and 10 wt % CNC binder) onto a carbon paper, using deionized water as a solvent (a small amount of ethanol was added for wetting), followed by vacuum drying at 60 °C for 12 h. CR2032 coin cells were assembled in an argon-filled glove box and performed on a LAND CT2001A battery tester in a voltage window of 1.8−2.6 V at room temperature. The electrolyte/sulfur ratios are 26 and 13 μL mg^{-1} for the Li−S cells with a sulfur loading of 4.1 and 8.5 mg cm^{-2}, respectively.

ASSOCIATED CONTENT

Supporting Information

The Supporting Information is available free of charge at https://pubs.acs.org/doi/10.1021/acsami.0c00537.

Length and diameter distribution of CNCs, viscosity comparison of the CMC binder and the CNC binder, SEM image and elemental mapping of the sulfur cathode with the CNC binder, SEM images of PP and CNC-coated separators, bending experiments of the CNC-coated separator and the sulfur electrode using the CNC binder, CV curves and CE of the Li−S battery with the CNC binder and the CNC-coated separator, and a comparison of the electrochemical performance of separator-related Li−S batteries (PDF)

AUTHOR INFORMATION

Corresponding Authors

Hui Wang − *Taishan Scholar Advantage and Characteristic Discipline Team of Eco-Chemical Process and Technology, State*

https://dx.doi.org/10.1021/acsami.0c00537
ACS Appl. Mater. Interfaces 2020, 12, 17592−17601

Key Lab Base of Eco-Chemical Engineering and School of Polymer Science and Engineering, Qingdao University of Science and Technology, Qingdao 266042, China; Email: h54wang@uwaterloo.ca

Lei Wang − *Taishan Scholar Advantage and Characteristic Discipline Team of Eco-Chemical Process and Technology, State Key Lab Base of Eco-Chemical Engineering and School of Chemistry and Molecular Engineering, Qingdao University of Science and Technology, Qingdao 266042, China*; orcid.org/0000-0001-7275-4846; Email: inorchemwl@126.com

Shanqing Zhang − *Centre for Clean Environment and Energy, Environmental Futures Research Institute, School of Environment and Science, Griffith University, Gold Coast, Queensland 4222, Australia*; orcid.org/0000-0001-5192-1844; Email: s.zhang@griffith.edu.au

Authors

Jie Liu − *Taishan Scholar Advantage and Characteristic Discipline Team of Eco-Chemical Process and Technology, State Key Lab Base of Eco-Chemical Engineering and College of Chemical Engineering, Qingdao University of Science and Technology, Qingdao 266042, China*; orcid.org/0000-0002-5402-1881

Yanyan Li − *Taishan Scholar Advantage and Characteristic Discipline Team of Eco-Chemical Process and Technology, State Key Lab Base of Eco-Chemical Engineering and School of Chemistry and Molecular Engineering, Qingdao University of Science and Technology, Qingdao 266042, China*; orcid.org/0000-0002-3572-1858

Yuxue Xuan − *Taishan Scholar Advantage and Characteristic Discipline Team of Eco-Chemical Process and Technology, State Key Lab Base of Eco-Chemical Engineering, Qingdao University of Science and Technology, Qingdao 266042, China*

Liujiang Zhou − *Theoretical Physics and Chemistry of Materials, Los Alamos National Laboratory, Los Alamos, New Mexico 87545, United States; Institute of Fundamental and Frontier Sciences, University of Electronic Science and Technology of China, Chengdu 610054, China*; orcid.org/0000-0001-5814-4486

Dong Wang − *Taishan Scholar Advantage and Characteristic Discipline Team of Eco-Chemical Process and Technology, State Key Lab Base of Eco-Chemical Engineering and School of Chemistry and Molecular Engineering, Qingdao University of Science and Technology, Qingdao 266042, China*

Zhenwei Li − *Taishan Scholar Advantage and Characteristic Discipline Team of Eco-Chemical Process and Technology, State Key Lab Base of Eco-Chemical Engineering and School of Chemistry and Molecular Engineering, Qingdao University of Science and Technology, Qingdao 266042, China*

Haifeng Lin − *Taishan Scholar Advantage and Characteristic Discipline Team of Eco-Chemical Process and Technology, State Key Lab Base of Eco-Chemical Engineering and School of Chemistry and Molecular Engineering, Qingdao University of Science and Technology, Qingdao 266042, China*

Sergei Tretiak − *Theoretical Physics and Chemistry of Materials, Los Alamos National Laboratory, Los Alamos, New Mexico 87545, United States; Skolkovo Institute of Science and Technology, Moscow 143026, Russia*; orcid.org/0000-0001-5547-3647

Ziyang Guo − *Taishan Scholar Advantage and Characteristic Discipline Team of Eco-Chemical Process and Technology, State Key Lab Base of Eco-Chemical Engineering and School of Chemistry and Molecular Engineering, Qingdao University of Science and Technology, Qingdao 266042, China*; orcid.org/0000-0002-2577-2512

Complete contact information is available at: https://pubs.acs.org/10.1021/acsami.0c00537

Author Contributions

J.L., Y.L., and Y.X. contributed equally. The manuscript was written through contributions of all authors. All authors have given approval to the final version of the manuscript.

Notes

The authors declare no competing financial interest.

■ ACKNOWLEDGMENTS

This work was financially supported by the National Natural Science Foundation of China (21801150, 21571112, 51572136, and 51802170), the Natural Science Foundation of Shandong Province (ZR2018LB008 and ZR2018BEM014), the Shandong Taishan Scholar Program, and the Special Fund Project to Guide Development of Local Science and Technology by Central Government. L.Z. and S.T. acknowledge support from the U.S. Department of Energy through the Los Alamos National Laboratory (LANL) Directed Research and Development funds (LDRD) program and Center for Integrated Nanotechnologies (CINT).

■ REFERENCES

(1) Hu, G.; Xu, C.; Sun, Z.; Wang, S.; Cheng, H.-M.; Li, F.; Ren, W. 3D Graphene-Foam-Reduced-Graphene-Oxide Hybrid Nested Hierarchical Networks for High-Performance Li-S Batteries. *Adv. Mater.* **2016**, *28*, 1603−1609.

(2) Chung, S.-H.; Chang, C.-H.; Manthiram, A. A Core-Shell Electrode for Dynamically and Statically Stable Li-S Battery Chemistry. *Energy Environ. Sci.* **2016**, *9*, 3188−3200.

(3) Chen, S.-R.; Zhai, Y.-P.; Xu, G.-L.; Jiang, Y.-X.; Zhao, D.-Y.; Li, J.-T.; Huang, L.; Sun, S.-G. Ordered Mesoporous Carbon/Sulfur Nanocomposite of High Performances as Cathode for Lithium-Sulfur Battery. *Electrochim. Acta* **2011**, *56*, 9549−9555.

(4) Zhang, S. S. Liquid Electrolyte Lithium/Sulfur Battery: Fundamental Chemistry, Problems, and Solutions. *J. Power Sources* **2013**, *231*, 153−162.

(5) Park, K.; Cho, J. H.; Jang, J.-H.; Yu, B.-C.; De La Hoz, A. T.; Miller, K. M.; Ellison, C. J.; Goodenough, J. B. Trapping Lithium Polysulfides of a Li-S Battery by Forming Lithium Bonds in a Polymer Matrix. *Energy Environ. Sci.* **2015**, *8*, 2389−2395.

(6) Wang, H.; Yang, Y.; Liang, Y.; Robinson, J. T.; Li, Y.; Jackson, A.; Cui, Y.; Dai, H. Graphene-Wrapped Sulfur Particles as a Rechargeable Lithium-Sulfur Battery Cathode Material with High Capacity and Cycling Stability. *Nano Lett.* **2011**, *11*, 2644−2647.

(7) Song, J.; Gordin, M. L.; Xu, T.; Chen, S.; Yu, Z.; Sohn, H.; Lu, J.; Ren, Y.; Duan, Y.; Wang, D. Strong Lithium Polysulfide Chemisorption on Electroactive Sites of Nitrogen-Doped Carbon Composites For High-Performance Lithium-Sulfur Battery Cathodes. *Angew. Chem., Int. Ed.* **2015**, *54*, 4325−4329.

(8) Huang, C.; Xiao, J.; Shao, Y.; Zheng, J.; Bennett, W. D.; Lu, D.; Saraf, L. V.; Engelhard, M.; Ji, L.; Zhang, J.; Li, X.; Graff, G. L.; Liu, J. Manipulating Surface Reactions in Lithium-Sulphur Batteries Using Hybrid Anode Structures. *Nat. Commun.* **2014**, *5*, 3015.

(9) Seh, Z. W.; Zhang, Q.; Li, W.; Zheng, G.; Yao, H.; Cui, Y. Stable Cycling of Lithium Sulfide Cathodes Through Strong Affinity with a Bifunctional Binder. *Chem. Sci.* **2013**, *4*, 3673−3677.

(10) Ling, M.; Zhang, L.; Zheng, T.; Feng, J.; Guo, J.; Mai, L.; Liu, G. Nucleophilic Substitution Between Polysulfides and Binders Unexpectedly Stabilizing Lithium Sulfur Battery. *Nano Energy* **2017**, *38*, 82−90.

(11) Liu, J.; Galpaya, D. G. D.; Yan, L.; Sun, M.; Lin, Z.; Yan, C.; Liang, C.; Zhang, S. Exploiting a Robust Biopolymer Network Binder for an Ultrahigh-Areal-Capacity Li-S Battery. *Energy Environ. Sci.* **2017**, *10*, 750−755.
(12) Liu, X.; Qian, T.; Liu, J.; Tian, J.; Zhang, L.; Yan, C. Greatly Improved Conductivity of Double-Chain Polymer Network Binder for High Sulfur Loading Lithium-Sulfur Batteries with a Low Electrolyte/Sulfur Ratio. *Small* **2018**, *14*, 1801536.
(13) Bhattacharya, P.; Nandasiri, M. I.; Lv, D.; Schwarz, A. M.; Darsell, J. T.; Henderson, W. A.; Tomalia, D. A.; Liu, J.; Zhang, J.-G.; Xiao, J. Polyamidoamine Dendrimer-Based Binders for High-Loading Lithium-Sulfur Battery Cathodes. *Nano Energy* **2016**, *19*, 176−186.
(14) Liu, J.; Sun, M.; Zhang, Q.; Dong, F.; Kaghazchi, P.; Fang, Y.; Zhang, S.; Lin, Z. A Robust Network Binder with Dual Functions of Cu^{2+} Ions as Ionic Crosslinking and Chemical Binding Agents for Highly Stable Li-S Batteries. *J. Mater. Chem. A* **2018**, *6*, 7382−7388.
(15) Liu, J.; Zhang, Q.; Sun, Y.-K. Recent Progress of Advanced Binders for Li-S Batteries. *J. Power Sources* **2018**, *396*, 19−32.
(16) Jin, Z.; Xie, K.; Hong, X.; Hu, Z.; Liu, X. Application of Lithiated Nafion Ionomer Film as Functional Separator for Lithium Sulfur Cells. *J. Power Sources* **2012**, *218*, 163−167.
(17) Huang, J.-Q.; Zhang, Q.; Peng, H.-J.; Liu, X.-Y.; Qian, W.-Z.; Wei, F. Ionic Shield for Polysulfides Towards Highly-Stable Lithium-Sulfur Batteries. *Energy Environ. Sci.* **2014**, *7*, 347−353.
(18) Bauer, I.; Thieme, S.; Brückner, J.; Althues, H.; Kaskel, S. Reduced Polysulfide Shuttle in Lithium-Sulfur Batteries Using Nafion-Based Separators. *J. Power Sources* **2014**, *251*, 417−422.
(19) Dong, Q.; Shen, R.; Li, C.; Gan, R.; Ma, X.; Wang, J.; Li, J.; Wei, Z. Construction of Soft Base Tongs on Separator to Grasp Polysulfides from Shuttling in Lithium-Sulfur Batteries. *Small* **2018**, *14*, 1804277.
(20) Tu, S.; Chen, X.; Zhao, X.; Cheng, M.; Xiong, P.; He, Y.; Zhang, Q.; Xu, Y. A Polysulfide-Immobilizing Polymer Retards the Shuttling of Polysulfide Intermediates in Lithium-Sulfur Batteries. *Adv. Mater.* **2018**, *30*, 1804581.
(21) Chen, H.; Ling, M.; Hencz, L.; Ling, H. Y.; Li, G.; Lin, Z.; Liu, G.; Zhang, S. Exploring Chemical, Mechanical, and Electrical Functionalities of Binders for Advanced Energy-Storage Devices. *Chem. Rev.* **2018**, *118*, 8936−8982.
(22) Ma, G.; Huang, F.; Wen, Z.; Wang, Q.; Hong, X.; Jin, J.; Wu, X. Enhanced Performance of Lithium Sulfur Batteries with Conductive Polymer Modified Separators. *J. Mater. Chem. A* **2016**, *4*, 16968−16974.
(23) Yu, B.-C.; Park, K.; Jang, J.-H.; Goodenough, J. B. Cellulose-Based Porous Membrane for Suppressing Li Dendrite Formation in Lithium-Sulfur Battery. *ACS Energy Lett.* **2016**, *1*, 633−637.
(24) Pan, R.; Xu, X.; Sun, R.; Wang, Z.; Lindh, J.; Edström, K.; Strømme, M.; Nyholm, L. Nanocellulose Modified Polyethylene Separators for Lithium Metal Batteries. *Small* **2018**, *14*, 1704371.
(25) Pavlin, N.; Hribernik, S.; Kapun, G.; Talian, S. D.; Njel, C.; Dedryvère, R.; Dominko, R. The Role of Cellulose Based Separator in Lithium Sulfur Batteries. *J. Electrochem. Soc.* **2019**, *166*, A5237−A5243.
(26) Kontturi, E.; Meriluoto, A.; Penttilä, P. A.; Baccile, N.; Malho, J.-M.; Potthast, A.; Rosenau, T.; Ruokolainen, J.; Serimaa, R.; Laine, J.; Sixta, H. Degradation and Crystallization of Cellulose in Hydrogen Chloride Vapor for High-Yield Isolation of Cellulose Nanocrystals. *Angew. Chem., Int. Ed.* **2016**, *55*, 14455−14458.
(27) Habibi, Y.; Lucia, L. A.; Rojas, O. J. Cellulose Nanocrystals: Chemistry, Self-Assembly, and Applications. *Chem. Rev.* **2010**, *110*, 3479−3500.
(28) Trache, D.; Hussin, M. H.; Haafiz, M. K. M.; Thakur, V. K. Recent Progress in Cellulose Nanocrystals: Sources and Production. *Nanoscale* **2017**, *9*, 1763−1786.
(29) Lu, P.; Hsieh, Y.-L. Preparation and Characterization of Cellulose Nanocrystals from Rice Straw. *Carbohydr. Polym.* **2012**, *87*, 564−573.
(30) Grishkewich, N.; Mohammed, N.; Tang, J.; Tam, K. C. Recent Advances in the Application of Cellulose Nanocrystals. *Curr. Opin. Colloid Interface Sci.* **2017**, *29*, 32−45.
(31) Neto, W. P. F.; Mariano, M.; Silva, I. S. V. D.; Silvério, H. A.; Putaux, J. L.; Otaguro, H.; Pasquini, D.; Dufresne, A. Mechanical Properties of Natural Rubber Nanocomposites Reinforced with High Aspect Ratio Cellulose Nanocrystals Isolated from Soy Hulls. *Carbohydr. Polym.* **2016**, *153*, 143−152.
(32) Sahlin, K.; Forsgren, L.; Moberg, T.; Bernin, D.; Rigdahl, M.; Westman, G. Surface Treatment of Cellulose Nanocrystals (CNC): Effects on Dispersion Rheology. *Cellulose* **2018**, *25*, 331−345.
(33) Huq, T.; Salmieri, S.; Khan, A.; Khan, R. A.; Le Tien, C.; Riedl, B.; Fraschini, C.; Bouchard, J.; Uribe-Calderon, J.; Kamal, M. R.; Lacroix, M. Nanocrystalline Cellulose (NCC) Reinforced Alginate Based Biodegradable Nanocomposite Film. *Carbohydr. Polym.* **2012**, *90*, 1757−1763.
(34) Cai, J.; Zhang, Z.; Yang, S.; Min, Y.; Yang, G.; Zhang, K. Self-Conversion Templated Fabrication of Sulfur Encapsulated Inside the N-Doped Hollow Carbon Sphere and 3D Graphene Frameworks for High-Performance Lithium-Sulfur Batteries. *Electrochim. Acta* **2019**, *295*, 900−909.
(35) Wang, H.; Sencadas, V.; Gao, G.; Gao, H.; Du, A.; Liu, H.; Guo, Z. Strong Affinity of Polysulfide Intermediates to Multi-Functional Binder for Practical Application in Lithium-Sulfur Batteries. *Nano Energy* **2016**, *26*, 722−728.
(36) Wang, Z.; Dong, Y.; Li, H.; Zhao, Z.; Wu, H. B.; Hao, C.; Liu, S.; Qiu, J.; Lou, X. W. Enhancing Lithium-Sulphur Battery Performance by Strongly Binding the Discharge Products on Amino-Functionalized Reduced Graphene Oxide. *Nat. Commun.* **2014**, *5*, 5002.
(37) Bao, W.; Liu, L.; Wang, C.; Choi, S.; Wang, D.; Wang, G. Facile Synthesis of Crumpled Nitrogen-Doped MXene Nanosheets as a New Sulfur Host for Lithium-Sulfur Batteries. *Adv. Energy Mater.* **2018**, *8*, 1702485.
(38) Gao, X.-T.; Xie, Y.; Zhu, X.-D.; Sun, K.-N.; Xie, X.-M.; Liu, Y.-T.; Yu, J.-Y.; Ding, B. Ultrathin MXene Nanosheets Decorated with TiO_2 Quantum Dots as an Efficient Sulfur Host toward Fast and Stable Li-S Batteries. *Small* **2018**, *14*, 1802443.
(39) Shen, X.; Qian, T.; Chen, P.; Liu, J.; Wang, M.; Yan, C. Bioinspired Polysulfiphobic Artificial Interphase Layer on Lithium Metal Anodes for Lithium Sulfur Batteries. *ACS Appl. Mater. Interfaces* **2018**, *10*, 30058−30064.
(40) Shen, X.; Li, Y.; Qian, T.; Liu, J.; Zhou, J.; Yan, C.; Goodenough, J. B. Lithium Anode Stable in Air for Low-Cost Fabrication of a Dendrite-Free Lithium Battery. *Nat. Commun.* **2019**, *10*, 900.
(41) Cheng, X.-B.; Huang, J.-Q.; Zhang, Q.; Peng, H.-J.; Zhao, M.-Q.; Wei, F. Aligned Carbon Nanotube/Sulfur Composite Cathodes with High Sulfur Content for Lithium-Sulfur Batteries. *Nano Energy* **2014**, *4*, 65−72.
(42) Fang, R.; Li, G.; Zhao, S.; Yin, L.; Du, K.; Hou, P.; Wang, S.; Cheng, H.-M.; Liu, C.; Li, F. Single-Wall Carbon Nanotube Network Enabled Ultrahigh Sulfur-Content Electrodes for High-Performance Lithium-Sulfur Batteries. *Nano Energy* **2017**, *42*, 205−214.
(43) Huang, J.-Q.; Liu, X.-F.; Zhang, Q.; Chen, C.-M.; Zhao, M.-Q.; Zhang, S.-M.; Zhu, W.; Qian, W.-Z.; Wei, F. Entrapment of Sulfur in Hierarchical Porous Graphene for Lithium-Sulfur Batteries with High Rate Performance from −40 to 60 °C. *Nano Energy* **2013**, *2*, 314−321.
(44) Xu, H.; Jiang, Q.; Zhang, B.; Chen, C.; Lin, Z. Integrating Conductivity, Immobility, and Catalytic Ability into High-N Carbon/Graphene Sheets as an Effective Sulfur Host. *Adv. Mater.* **2019**, *32*, 1906357.
(45) Rana, M.; Ahad, S. A.; Li, M.; Luo, B.; Wang, L.; Gentle, I.; Knibbe, R. Review on Areal Capacities and Long-Term Cycling Performances of Lithium Sulfur Battery at High Sulfur Loading. *Energy Storage Mater.* **2019**, *18*, 289−310.

https://dx.doi.org/10.1021/acsami.0c00537
ACS Appl. Mater. Interfaces 2020, 12, 17592−17601

(46) Peng, H.-J.; Huang, J.-Q.; Cheng, X.-B.; Zhang, Q. Review on High-Loading and High-Energy Lithium-Sulfur Batteries. *Adv. Energy Mater.* **2017**, *7*, 1700260.
(47) Frisch, M. J.; Trucks, G. W.; Schlegel, H. B.; Scuseria, G. E.; Robb, M. A.; Cheeseman, J. R.; Scalmani, G.; Barone, V.; Petersson, G. A.; Nakatsuji, H.; Li, X.; Caricato, M.; Marenich, A. V.; Bloino, J.; Janesko, B. G.; Gomperts, R.; Mennucci, B.; Hratchian, H. P.; Ortiz, J. V.; Sonnenberg, J. L.; Williams-Young, D.; Ding, F.; Lipparini, F.; Egidi, F.; Goings, J.; Peng, B.; Petrone, A.; Henderson, T.; Ranasinghe, D.; Zakrzewski, V. G.; Gao, J.; Rega, N.; Zheng, G.; Liang, W.; Hada, M.; Ehara, M.; Toyota, K.; Fukuda, R.; Hasegawa, J.; Ishida, M.; Nakajima, T.; Honda, Y.; Kitao, O.; Nakai, H.; Vreven, T.; Throssell, K.; Montgomery, J. A., Jr.; Peralta, J. E.; Ogliaro, F.; Bearpark, M. J.; Heyd, J. J.; Brothers, E. N.; Kudin, K. N.; Staroverov, V. N.; Keith, T. A.; Kobayashi, R.; Normand, J.; Raghavachari, K.; Rendell, A. P.; Burant, J. C.; Iyengar, S. S.; Tomasi, J.; Cossi, M.; Millam, J. M.; Klene, M.; Adamo, C.; Cammi, R.; Ochterski, J. W.; Martin, R. L.; Morokuma, K.; Farkas, O.; Foresman, J. B.; Fox, D. J. *Gaussian 16*, Revision B.01; Gaussian, Inc.: Wallingford CT, 2016.

https://dx.doi.org/10.1021/acsami.0c00537
ACS Appl. Mater. Interfaces 2020, 12, 17592−17601